ISBN: 978-3-95450-207-3 doi:10.18429/JACoW-MEDSI2018-WEPH14

OPTOMECHANICAL OPTIMIZATION FOR A SAGITALLY BENT DOUBLE CRYSTAL MONOCHROMATOR, USING FINITE ELEMENTS AND RAY TRACING

N.Jobert†, T. Moreno, M.Ribbens, E.Fonda, Synchrotron SOLEIL, Gif Sur Yvette, FRANCE

Abstract

Designing a second crystal for a sagitally bent Double Crystal Monochromator (DCM) requires dealing with a number of conflicting requirements. Especially when working with high-energy photons, the angular aperture (Darwin width) becomes very narrow (below 10 µrad for Si) while simultaneously the bending radius is decreasing (down to 1.2 m for typical beamline dimensions at 40 keV). In this situation, the cross-talk between tangential and sagittal curvature becomes a key parameter, and two strategies are generally used to overcome the issue: either using a flat crystal with a specific length/width ratio, or usage of a rib-stiffened crystal. In the frame of the upgrade of the SAMBA beamline DCM, both solutions have been explored, using a suite of scripts connecting a general purpose FEM code (ANSYS) and a ray-tracing code (SpotX). This has allowed a systematic evaluation of a wide number of configurations, giving insight in the interaction between geometric parameters, and ultimately resulting in a significant increase in the photon throughput at 30 keV without comprising neither spectral resolution nor spot size at sample location.

INTRODUCTION

During the upgrade of the SAMBA (Spectroscopy Applied to Material Based Absorption) beamline DCM, the second crystal needed to be replaced, along with its bending mechanics. Two improvements were requested by the beamline scientist. Firstly, it was desired to extend the 2 nd crystal usable length so that the corresponding (longitudinal) translation stage could be removed, thus improving mechanical stability. Secondly, the photon throughput at high energies had to be as high as possible (preferably no less than 50% at 30 keV).

OBJECTIVES

The beamline layout is provided in Fig. 1. Combining the Bragg law for first order diffraction (eq. 1) and the equation for sagittal focusing (eq.2), the linear relationship between sagittal curvature and energy is derived (eq. 3).

$$2\,d\sin\left(\theta_{Bragg}\right)=\lambda \qquad \text{(eq. 1)}$$

$$\frac{1}{p}+\frac{1}{q}=\frac{2\sin(\theta)}{\rho} \qquad \text{(eq.2)}$$

$$\rho\,E=cte=\left(\frac{hc}{d}\,\frac{pq}{p+q}\right) \qquad \text{(eq.3)}$$

Where, d is the spacing between crystal planes, λ is the wavelength, h is Planck constant, c is the light celerity, p and q are the object and image distances, ρ is the sagittal bending radius, E is the photons working energy.

A Si(220) monocrystal is used, so that the Bragg Angle and the curvature in the 5-40 keV energy range are as follows (Fig. 2):

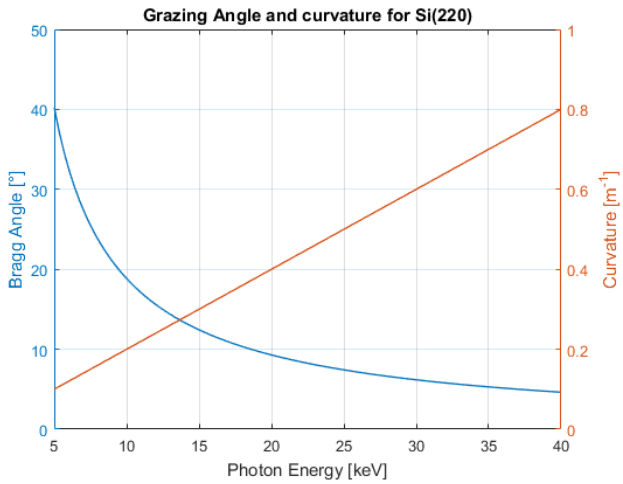

Figure 2: Bragg Angle and curvature.

In order to lose a minimal amount of photons, the parallelism between the first and the second crystals must remain well below the Darwin with of the crystal, which becomes increasingly small at high energies :

- @20keV: 9.3 µrad
- @30keV: 6.2 µrad
- @40keV: 4.6 µrad

Since the footprint has a length of about 10 to 20 mm, meeting the slope error criterion makes it necessary to have longitudinal bending radius larger than 1000 m. Compared to the sagittal curvature (slightly above 1 m), this in turn requires achieving a decoupling ratio of 1000 and above. The anticlastic effect must therefore be drastically minimized.

†nicolas.jobert@synchrotron-soleil.fr

ISBN: 978-3-95450-207-3 doi:10.18429/JACoW-MEDSI2018-WEPH14

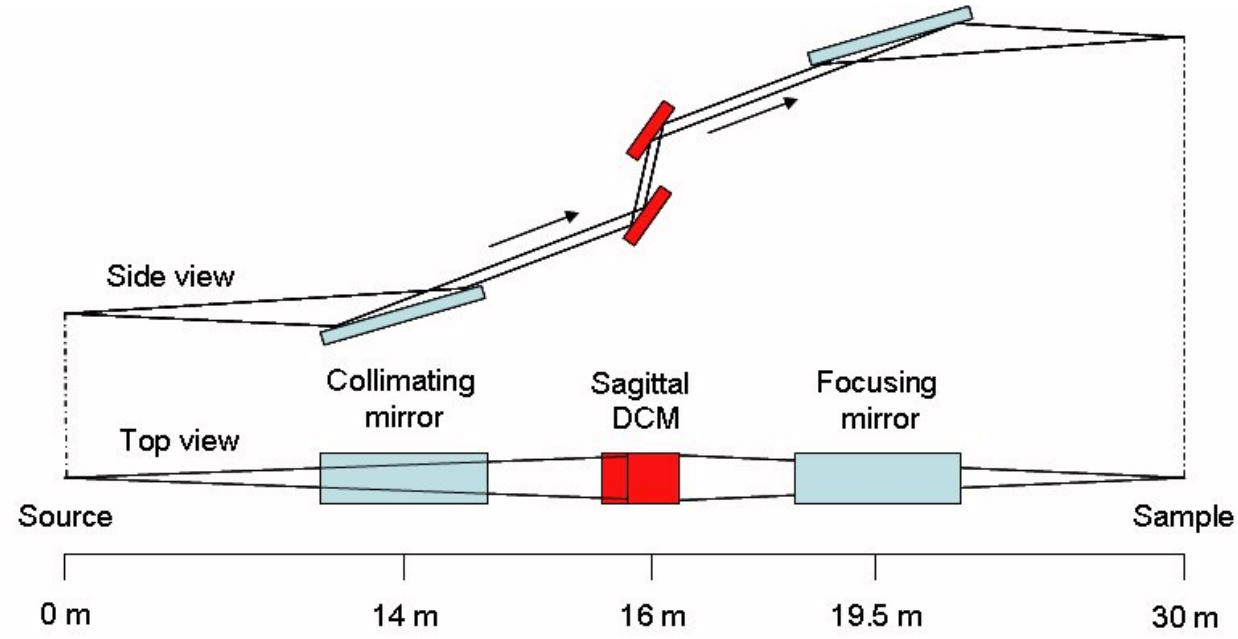

Figure 1: SAMBA Beamline Layout (simplified).

METHODS AND RESULTS

In order to achieve such a decoupling, we rely on two well known methods. The first is the introduction of ribs in order to increase the crystal longitudinal bending stiffness, while keeping the transverse bending stiffness unmodified [1]. The second is the usage of a flat crystal with a specific length to width ratio [2].

Because of the relatively large design space, a numerical Design Of Experiment (DOE) approach has been used, the 4 parameters being the crystal width and length and ribs spacing and height. For each parameter, 3 values have been used (low, base, high), resulting in a 3^4 DOE. Moreover, the results needed to be obtained for various photon energies and beam position along the crystal length, hence a systematic and efficient approach was required.

Mechanical Generation and Analysis

ANSYS Parametric Design Language (APDL) scripts have been written to generate, solve, and post process the results for each design, at 3 working energies (5, 20 and 30 keV).

The bender mechanism is supposed to be free of parasitics, perfectly stiff, and the connection effective on both sides of the jaws. Bender mechanism (virtual) rotation axes are placed so as to avoid overstressing the mirror.

All models use brick elements with mid side nodes, hence the shape functions are parabolic. In order to capture the local bending radius variation due to the presence of the ribs, two elements through thickness have been employed (Fig. 3 and Fig. 4). Analysis are conducted using linear material model and isotropic properties (Poisson ratio ν=0.27).

Each model is labelled using a 4 digits code:

- digit1: width (1,2,3=30,40,50 mm)
- digit2: length (1,2,3=90,100,110 mm)
- digit3: rib height (0=flat, 1,2,3=5,7,9 mm)
- digit4: thickness (1,2,3=0.5, 0.7, 0.9 mm)

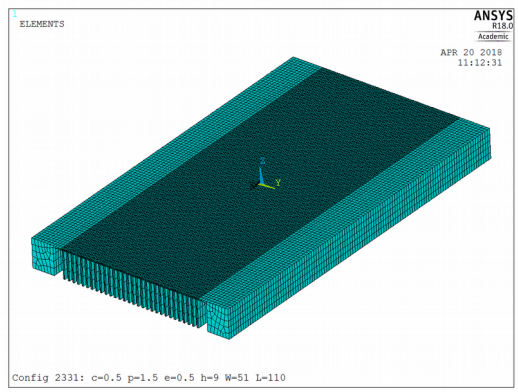

Figure 3: Ribbed design FEM.

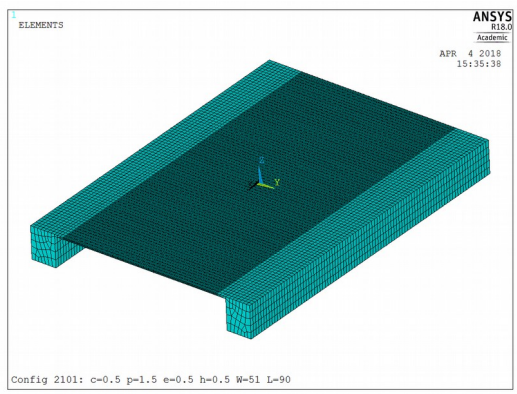

Figure 4: Flat design FEM.

ISBN: 978-3-95450-207-3 doi:10.18429/JACoW-MEDSI2018-WEPH14

Optical Surface Defect Assessment

Deformed shapes are read into Matlab, then the best fit cylinder is obtained and subtracted, giving the geometric *defect*. Then, for each working energy and each working position the following quantities are determined:

- Ratio of the footprint for which longitudinal slope is within Darwin Width
- RMS deviation of the sagittal bending radius.

Then the two best configurations (in terms of photon throughput) are selected (Fig. 5)

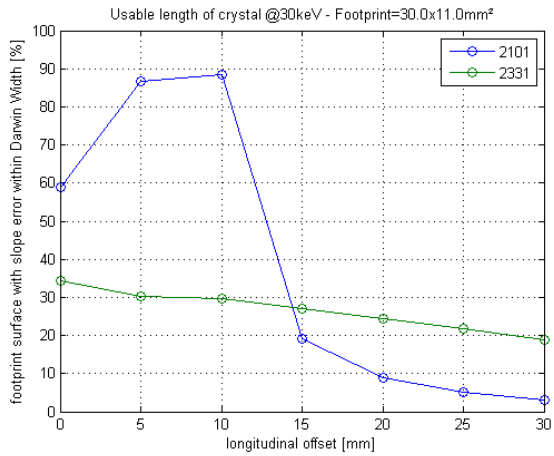

Figure 5: Photon throughput at various distances from the crystal centerline.

It clearly appears from the estimation of the slopes that the ribbed design has a nearly homogeneous anticlastic bending ratio along the length (of about 500 m, see Fig. 6), while the flat design has a saddle point near the centre (Fig. 7).

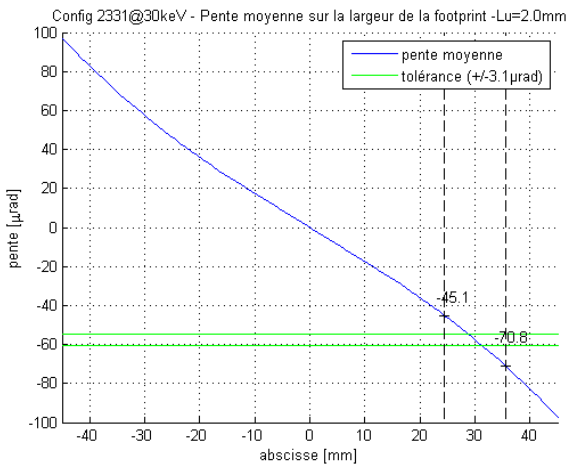

Figure 6: Longitudinal slope error for the ribbed design.

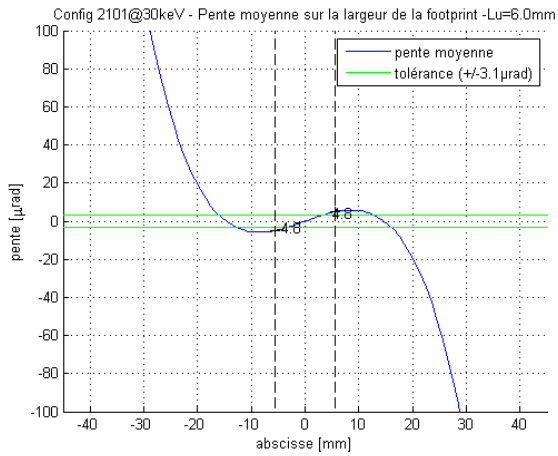

Figure 7: Longitudinal slope error for the flat design.

It must be acknowledged that those conclusions, based on purely geometric quantities, are only approximations since two effects are missing. Firstly, the anticlastic effect will not only reduce the photon throughput, it will also induce a vertical defocusing effect. Secondly, the defocusing effect of the local variation of sagittal bending radius cannot be readily estimated using such a simple indicator as the RMS bending radius (about 3% for the ribbed design, and virtually negligible for the flat design). Also, the effect of the source vertical divergence is not accounted for, and it is likely that the apparent increase in photon throughput will be somehow reduced by this effect. Therefore, to reach a consolidated conclusion, one needs to use a dedicated optical tool for X-rays.

Validation using Ray Tracing Calculations

A complete optical model of the beamline is built using the SpotX software [3]. The analysis includes the source (Bending Margnet), a Be filter, vertical collimating and focusing mirrors, along with their optical properties. Then the analysis is executed based on ray tracing algorithm and a Monte Carlo method.

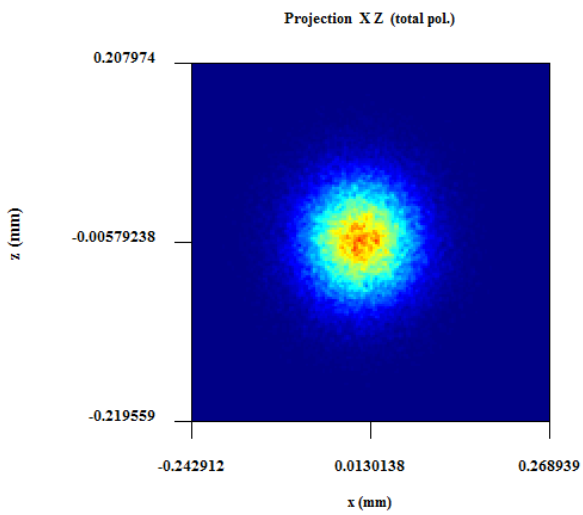

Figure 8: Projection of photon flux @30keV.

ISBN: 978-3-95450-207-3 doi:10.18429/JACoW-MEDSI2018-WEPH14

At first, no geometric defect on the 2nd crystal is accounted for, this configuration serves as a reference. Then, the optical defect for the two most promising configurations are included, and the analysis is repeated. Case "Opt1" corresponds with the optimal configuration using ribs, while case "Opt2" corresponds with a flat design. The raw data consists of a 2D map of photon flux obtained at the sample location which is shown in Fig. 8. Beam horizontal and vertical profiles are provided in Fig. 9 and Fig. 10.

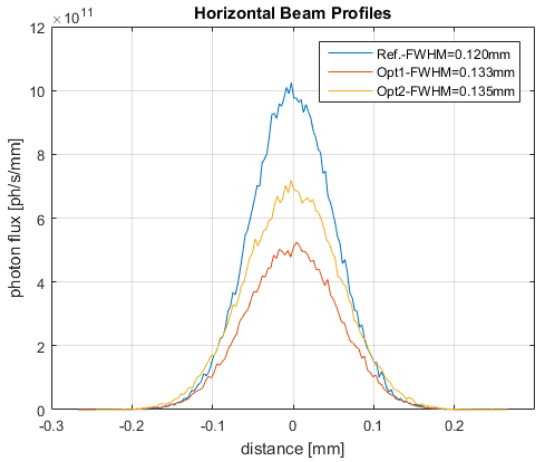

Figure 9: Horizontal Beam Profiles.

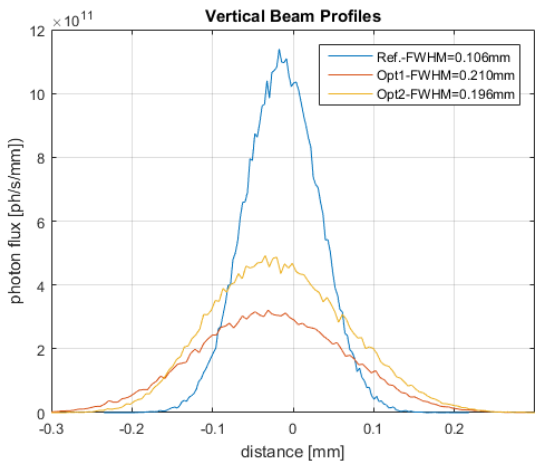

Figure 10: Vertical Beam Profiles.

For each case, one estimates the footprint dimensions (Full Width at Half Maximum), the energy resolution, and the total photon flux. Results are compiled in Table 1.

Both optimal designs are compliant with the initial request, but the Option 2 (flat design) reach 80% of photon throughput, to be compared with 60% for the ribbed design (Option1). In both cases, horizontal focusing and energy are almost not affected, while the vertical focusing is clearly degraded.

Table 1: Optical Figures of Merit

Case	FWHM (H/V) (µm)		FWHM (eV)	Flux (10^{10}ph/s)
Ref.	120	105	2.55	12.8
Opt1	138	206	2.62	7.2
Opt2	129	219	2.79	10.1
Target	<150	<300	<3.0	>6.4

CONCLUSIONS AND OUTLOOK

Using a DOE approach, it was shown that a substantial increase in photon throughput was possible, by minor modifications of the crystal geometric features:

- The ribbed design provides nearly homogeneous flatness along the length, while the flat design is only usable when the beam centre is located less than 10mm away from mirror axis
- When beam footprint is longitudinally centred on the crystal, flat design is significantly superior. This comes at the price of needing a dedicated translation
- For the ribbed design, aberrations due to the local variation of the bending radius ("microlenses" effect) were found to be insignificant at the focus position

Two major simplifications have been made. Firstly, FE analyses have been executed neglecting geometric non linearities, which is acceptable because of the bending radius being larger than the crystal width (R/W> 30 @30keV). However, because of the high accuracy typically required for optical calculations, taking into account those second order effect might be required, especially since high fidelity is required at those higher energies. Secondly, monocrystal anisotropic behaviour has been discarded, which could slightly modify the results [4].

Finally, the performance of the crystal will somehow be degraded due to the defects induced by the gluing process and the bender geometric imperfections and parasitics. Thermal/mechanical/optical simulations will be employed to estimate their severity and make corrections as required.

REFERENCES

[1] C. J. Sparks, G.E. Ice, J. Wong and B.W. Batterman, "Sagittal focusing of synchrotron x-radiation with curved crystals", in *Nucl. Instrum. Methods,* 1982, **194** 73,

[2] Mikhail Antimonov, Ali Khounsary "On the influence of monochromator thermal deformations on X-ray focusing", in *J. Phys. Conf. Ser.,* 2014, **493** 012003

[3] T. Moreno, & M. Idir, "SPOTX a ray tracing software for X-ray optics", in *J. Phys.,* 2001, IV Fr. **11**, 527–531.

[4] L. Zhang, "Anisotropic elasticity of silicon and its application to the modelling of X-ray optics", in *J. Synchrotron Radiation* 2014 May 1; 21(Pt 3): 507–517.